A&A 600, A42 (2017)
DOI: 10.1051/0004-6361/201629784

Astronomy & Astrophysics

The structure of critically-rotating accreting stars

H. F. Song[1,2,5], J. Z. Wang[3,1], F. Song[4,5], and J. T. Wang[1]

[1] College of Physics, Guizhou University, Guiyang, 550025 Guizhou Province, PR China
e-mail: hfsong@gzu.edu.cn; songhanfeng@163.com
[2] Geneva Observatory, University of Geneva, 1290 Sauverny, Switzerland
[3] School of Physics and Electronic Engineering, Kaili University, Kaili, 556011 Guizhou Province, PR China
[4] College of Science, Jimei University, Xiamen city, 361021 Fujian Province, PR China
[5] Key Laboratory for the Structure and Evolution of Celestial Objects, Chinese Academy of Sciences, 650011 Kunming, PR China

Received 25 September 2016 / Accepted 17 December 2016

ABSTRACT

Context. The structure characteristics of the critically-rotating accretor in binaries are investigated in this paper, on the basis of the potential function including rotational and tidal distortions.
Aims. Our aim is to investigate the structure of the accretor when the accreting star reaches the critical velocity.
Methods. In this paper, we have implemented the prescription described by Kippenhahn & Thomas (1970, Proc. IAU Colloq., 4, 20) and Landin et al. (2009, A&A, 494, 209).
Results. The traditional model merely included the hydrodynamical effect of rotation. When comparing this model with ours, we find that it is very necessary for the rapidly rotating accreting star to include the gravitational potentials from tides $\Psi_{\rm tide}$, and the distortions of the star resulting from rotation $\Psi_{\rm dis,rot}$. Furthermore, we find that the mean effective gravitational acceleration can be decreased in the distort model, and the star shifts towards low temperature and low luminosity. Rotation and tides can extend the convection zone below the surface, and reduce the convective core in the center of stars due to the Solberg-Hoiland criterion. Rotational distortions derived from $\Psi_{\rm dis,rot}$ can intensify the critical velocity whereas the tide force derived from $\Psi_{\rm tide}$ tends to reduce the critical velocity. Rapid rotation induced by mass transfer also causes the central temperature to decrease, and triggers efficient mixing which can significantly modify the H-profile.

Key words. binaries : close – stars: rotation – stars: evolution – stars: massive

1. Introduction

It is well known that rotation is regarded as a very important factor that needs to be considered to investigate the evolution of the massive star (Heger et al. 2000; Meynet & Maeder 2000; Maeder & Meynet 2012; Langer 2012). The centrifugal force changes the stellar shape from sphere to spheroid. The equatorial radius can be about 1.5 times larger than the polar radius according to Roche approximation when the stars approach the break-up rotation (Georgy et al. 2011). As a result of the deformation of the star, the radiative energy flux and the effective temperature vary with the latitude (von Zeipel 1924). Rotation can drive various mixing processes in the stellar interior and rotational mixing is probably the most important effect in massive stars (Meynet et al. 2006, 2010; Mathis & Zahn 2004; Mathis et al. 2004; Zahn 1992). Meridional circulations and shear turbulence dominate rotationally induced mixing in massive stars, and transfer both angular momentum and chemical species (Maeder & Zahn 1998; Talon & Zahn 1997; Maeder 2003). Fresh nitrogen thus appears at the surface of the star and becomes continuously more enriched as function of time during core-hydrogen burning (Maeder & Meynet 2000b).

In a rotating binary system, the joint effect of rotation and tides modifies the shapes of two components from the perfect sphere to triaxial ellipsoids (Landin et al. 2009; Song et al. 2009, 2011; Huang 2004). Eggleton & Kiseleva (1998) have presented the equations governing the quadrupole tensor of a star distorted both by rotation and by the presence of a companion in a possibly eccentric orbit. During the evolution of massive binaries, mass and angular momentum are transferred from the donor to the recipient during Roche lobe overflow (RLOF). Rapid mass transfer can spin up an accreting star to critical rotation (Packet 1981; Langer et al. 2003; Langer 2012). In the present work, we aim to investigate for the first time how the deformation of stars can be induced by both rotation and tide at critical rotation. In particular, we aim to discover how the critical rotation modifies the structure and evolution of the accreting star.

The paper is organized as follows: the potential function which included the combined effects of rotational and tidal distortions, and the structure equations of rotating binaries are given in Sect. 2. Various torques that affect the accreting star are introduced in Sect. 3. In Sect. 4, the result of numerical calculations are described and discussed in detail. And finally in Sect. 5, conclusions are made.

2. The potential function and the rotating stellar structure equations

2.1. The potential function including the rotational and tidal distortions

We consider a close binary consisting of two stars with masses M_1 and M_2 in a circular orbit with orbital period $P_{\rm orb}$, let a be the orbital separation. A coordinate system $\mathcal{R}_E$ rotating with the spin angular velocity of the secondary star M_2 is introduced (cf. Fig. 1). The mass center of the secondary star M_2 is regarded as

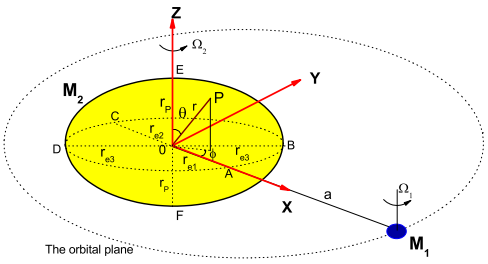

Fig. 1. Spherical coordinates system associated with the equatorial reference frame $\mathcal{R}_E$:O,X,Y, Z of an extended body M_2; We have $\boldsymbol{r}_p = (\boldsymbol{r}, \theta, \varphi)$. The spin of M_2 is perpendicular to the orbital plane. The dashed line illustrates the orbit of M_1.

the origin. It is presumed that the z-axis is perpendicular to the orbital plane, and the positive x-axis penetrates the mass center of the primary star M_1. The two stars rotate with angular velocity Ω_1 and Ω_2 around an axis perpendicular to the orbital plane.

If the coordinates of the point P are the radius r, the polar angular θ, and the azimuthal angle ϕ, then the total potential in the stellar interior (to first-order approximation) consists of five parts (Kopal 1960, 1974; Endal & Sofia 1976; Landin et al. 2009): the spherical symmetric part of the gravitational potential, $\psi_{\rm grav}$, the cylindrically symmetric potential due to rotation, $\psi_{\rm rot}$, the potential due to tides $\psi_{\rm tide}$, and the non-symmetric part of the gravitational potential due to the distortion of the star resulting from rotation, $\psi_{\rm dis,rot}$ and tides $\psi_{\rm dis,tide}$. This total potential is written as

$$\begin{aligned}\Psi &= \psi_{\rm grav} + \psi_{\rm rot} + \psi_{\rm tide} + \psi_{\rm dis,rot} + \psi_{\rm dis,tide}\\ &= \frac{GM_\psi}{r} + \frac{1}{2}\Omega_2^2 r^2 \sin^2\theta + \frac{GM_1}{a}\left[1 + \sum_{j=2}^{4}\left(\frac{r_0}{a}\right)^j P_j(\lambda)\right]\\ &\quad - \frac{4\pi}{3r^3}P_2(\cos\theta)\int_0^{r_0}\rho\frac{r_0'^7}{M_\psi}\Omega_2^2\frac{5+\eta_2}{2+\eta_2}{\rm d}r_0'\\ &\quad + 4\pi G M_1\sum_{j=2}^{4}\frac{P_j(\lambda)}{(ra)^{j+1}}\int_0^{r_0}\rho\frac{r_0'^{2j+3}}{M_\psi}\frac{j+3+\eta_j}{j+\eta_j}{\rm d}r_0',\end{aligned} \tag{1}$$

where r and Ω_2 are respectively the radius and the spin angular velocity of the rotating star 2, $\lambda = \cos\varphi\sin\theta$, and $P_j(\lambda)$ are the jth-order Legendre polynomials. ψ_r and ψ_t are, respectively, the potential functions which are induced by rotation ($\psi_r = \psi_{\rm rot} + \psi_{\rm dis,rot}$), and tide ($\psi_t = \psi_{\rm tide} + \psi_{\rm dis,tide}$). In Eq. (1) above, the quantities η_j are of particular importance for our research. They can be derived from the Radau´s differential equation with a 4th-order Runge-Kutta method (Press et al. 1992)

$$r\frac{{\rm d}\eta_j}{{\rm d}r} + 6\frac{\rho(r)}{\bar\rho(r)}(\eta_j+1) + \eta_j(\eta_j-1) = j(j+1), \tag{2}$$

where $\eta_j(0) = j - 2 (j = 2, 3, 4)$, $\rho(r)$ is the local density at a distance r from the center, and $\bar\rho(r)$ is the mean density within inner sphere of radius r.

2.2. The correction factors in the rotating stellar model

Adopting the Kippenhahn and Thomas method, we can define the mean quantities as $\langle g_{\rm e}\rangle$ and $\langle g_{\rm e}^{-1}\rangle$. These are the values of effective gravity and its opposite values over the isobar surface (Kippenhahn & Thomas 1970),

$$\langle g_{\rm e}\rangle = \frac{1}{S_\Psi}\int_{S_\Psi} g(r,\theta,\phi){\rm d}\sigma, \tag{3}$$

$$\langle g_{\rm e}^{-1}\rangle = \frac{1}{S_\Psi}\int_{S_\Psi}\frac{1}{g(r,\theta,\phi)}{\rm d}\sigma, \tag{4}$$

where $S_\Psi = \int_{S_\Psi}{\rm d}\sigma$, the mass inside the equipotential surfaces is M_Ψ and luminosity is L_Ψ. The equipotential surface has the area of S_Ψ, and r_Ψ is the radius of the topological equivalent sphere with the same volume V_Ψ. We note that the local effective gravity $\boldsymbol{g}_{\rm e}$ has three components which have been derived from Eqs. (A.7)–(A.9). The quantity ${\rm d}\sigma$ can be derived from Eq. (A.26).

The correction factors in the rotating stellar model are written as

$$f_p = \frac{4\pi r_\Psi^4}{GM_\Psi S_\Psi}\frac{1}{\langle g_{\rm e}^{-1}\rangle}, \tag{5}$$

$$f_t = \left(\frac{4\pi r_\Psi^2}{S_\Psi}\right)^2\frac{1}{\langle g_{\rm e}\rangle\langle g_{\rm e}^{-1}\rangle}. \tag{6}$$

In the case of isolated and non-rotating stars, we have used $f_p = f_t = 1$. Using the lowest approximation, the correction factors are treated as $f_p = 1 - \frac{2\Omega^2 R}{3GM}$ and $f_t = 1$ in the traditional rotating model which merely included the hydrodynamical effect of rotation (Kähler 1986).

2.3. The temperature gradients and Solberg-Hoiland criterion for stability

The effect of rotation and tides on the temperature gradient has been included in our computations. They are given by

$$\nabla_{\rm rad} = \frac{3}{16\pi acG}\frac{\kappa L_P P}{M(r)T^4}\frac{f_t}{f_p}, \tag{7}$$

$$\nabla_{\rm ad} = \frac{8-6\beta}{32-24\beta-3\beta^2}, \tag{8}$$

where $\nabla_{\rm rad}$ and $\nabla_{\rm ad}$ are the radiative temperature gradient and the adiabatic gradient, respectively, the quantity $\beta = \frac{P_{\rm g}}{P}$ is the ratio of gas pressure to the total pressure. A fluid element displaced in a rotating star is also subject to the restoring effect of angular momentum conservation (Kippenhahn & Weigert 1990). This leads to the Solberg-Hoiland criterion for stability, in which

$$\nabla_{\rm ad} + \nabla_\Omega\langle\sin\theta\rangle - \nabla_{\rm rad} > 0, \tag{9}$$

with

$$\nabla_\Omega = 4\frac{\Omega^2}{g_{\rm grav}}\frac{H_P}{\delta} = \frac{4\Omega^2}{g_{\rm grav}\rho}\frac{P}{g_{\rm e}\delta} \tag{10}$$

for constant angular velocity (Maeder et al. 2008). Here $g_{\rm grav}$ is the self gravity and H_p designates as the pressure scale height. In one-dimensional stellar model, the quantity $\langle\sin\theta\rangle$ has a value of ~0.75.

2.4. Expressions of the critical velocity

The high distortion which is induced by rapid rotation and tides has an important impact on the critical velocity. When a rotating star of mass M_2, and spin angular velocity Ω_2 is in the binary

system, the total gravity is the sum of the gravitational, centrifugal, and tidal accelerations:

$$\boldsymbol{g}_{\rm tot} = \boldsymbol{g}_{\rm grav} + \boldsymbol{g}_{\rm rot} + \boldsymbol{g}_{\rm tide} + \boldsymbol{g}_{\rm dis,rot} + \boldsymbol{g}_{\rm dis,tide}. \quad (11)$$

The critical angular velocity $\Omega_{\rm c,1}$ corresponds to the angular velocity at equator of the star such that the centrifugal force balances the gravity exactly. The classical critical angular velocity or the $\Omega-$ limit (to distinguish it from the $\Omega\Gamma$ limit as defined in Maeder & Meynet 2000) can be given by the equation,

$$g_r\left(R_{\rm eb}, \frac{\pi}{2}, 0\right) = 0 \quad (12)$$

where the quantity $R_{\rm eb}$ denotes the equatorial radius at the break-up velocity, the critical velocity is $v_{\rm crit,1} = R_{\rm eb}\Omega_{\rm crit}$. The quantity $\Omega_{\rm crit}$ is the critical angular velocity.

2.5. The transport equation for angular momentum

The transport of the angular momentum can be treated as a diffusion process (Endal & Sofia 1978; Pinsonneault et al. 1989). The equation can be written as (Heger et al. 2000)

$$\left(\frac{\partial\Omega}{\partial t}\right)_m = \frac{1}{i}\left(\frac{\partial}{\partial m}\right)_t\left[(4\pi r^2\rho)^2 i\nu\left(\frac{\partial\Omega}{\partial m}\right)_t\right] - \frac{2\Omega}{r}\left(\frac{\partial r}{\partial t}\right)_m\left(\frac{1}{2}\frac{{\rm dln}\, i}{{\rm dln}\, r}\right), \quad (13)$$

where ν is the turbulent viscosity which includes various instabilities ($\nu = D_{\rm conv} + D_{\rm sem} + D_{\rm DSI} + D_{\rm SHI} + D_{\rm SSI} + D_{\rm ES} + D_{\rm GSF}$), and i is the specific angular momentum of a shell at mass coordinate m. The final term in the above equation (an advection term) accounts for contraction or expansion of the layers at constant mass coordinate.

2.6. The transport of the chemical elements

The diffusion equation of the chemical elements can be given by (Heger et al. 2000)

$$\left(\frac{\partial y_\alpha}{\partial t}\right) = \frac{1}{\rho r^2}\frac{\partial}{\partial r}\left[\rho r^2 D_{\rm dif}\left(\frac{\partial y_\alpha}{\partial r}\right)\right] + \left(\frac{\partial y_\alpha}{\partial t}\right)_{\rm nuc}, \quad (14)$$

where $(\frac{\partial y_\alpha}{\partial t})_{\rm nuc}$ is a source term from nuclear reactions, and y_α is the relative abundance of αth nuclide. Meridional circulations are the main physical process which can mix the chemical elements in a solid-body rotating star. The diffusion coefficient due to meridional circulations can be used as $D_{\rm dif} \equiv \min\{d_{\rm inst}, H_{v,\rm ES}\}U_2(r)$. $d_{\rm inst}$ and $H_{v,\rm ES}$ denote the extent of the instability and the velocity scale height, respectively. We currently use an approximate formula for meridional circulations by Maeder & Zahn (1998),

$$U_2(r) = \frac{L}{M_{\rm e}g_{\rm e}}\frac{P}{C_p\rho T}\frac{1}{\nabla_{\rm ad} - \nabla_r + \nabla_\mu} \times\left(1 - \frac{\epsilon}{\epsilon_m} - \frac{\Omega^2}{2\pi G\rho}\right)\frac{4\Omega^2 r^3}{3Gm}, \quad (15)$$

where $M_{\rm e} = m(1 - \frac{\Omega^2}{2\pi G\rho})$, the quantity $\epsilon = E_{\rm nuc} + E_{\rm grav}$ is the total local energy emission, the quantity ϵ_m is L/m, C_p is the specific heat capacity at constant pressure. The thermodynamic ratio $\frac{\gamma}{\delta}$ used by Maeder & Zahn (1998) is set to unity. This is correct for a perfect gas. We have also approximated the factor $\frac{\tilde{g}}{g}$ of Zahn (1992) by $\frac{4\Omega^2 r^3}{3Gm}$. The description of angular momentum transport and rotational mixing in massive stars is given in the references (Maeder & Meynet 2000b; Rieutord 2006; Decressin et al. 2009). The diffusive approach is only a first step for such complex modeling.

3. The spin-up and spin-down mechanisms of the accreting star

The mass-transfer rate from star 1 to star 2 during RLOF is

$$\dot{M}_{1R} = -C\cdot(\log R_1/R_L)^3, \quad (16)$$

where the quantity C is set to 1.0×10^4 $M_\odot$/yr. For Roche-lobe radius R_L, we use Eggleton's (1983) analytic expression. During the evolution of massive binaries, mass and angular momentum are transferred from the donor to the recipient during RLOF. Rapid mass transfer can spin up an accreting star to critical rotation (Packet 1981; Langer 2012).

By comparing the radius of the accreting star $R_{\rm A}$ to the minimum distance $R_{\rm min}$ of the stream from the centre of the gainer, we determined whether disk accretion, when $R_{\rm A} < R_{\rm min}$ or direct impact accretion, when $R_{\rm A} > R_{\rm min}$, occurs. According to Ulrich & Burger (1976), the quantity $R_{\rm min}$ can be calculated by $R_{\rm min} \approx 0.0425a[q(1+q)]^{1/4}$. The quantity q is the mass ratio of the companion to the considered star. The variation of spin angular momentum of the accreting star can be expressed as

$$\frac{{\rm d}J_2}{{\rm d}t} = \dot{J}_{\rm mt} + \dot{J}_{\rm tide} - \dot{J}_{\rm wind}, \quad (17)$$

where J_2 is the spin angular momentum of the accreting star, $\dot{J}_{\rm mt}$ is the torque due to mass transfer, $\dot{J}_{\rm wind}$ is the wind torque, $\dot{J}_{\rm tide}$ is the tide torque. The spinning-up of the gainer due to RLOF is characterized by an enhancement of its rotational angular momentum $\dot{J}_{\rm mt}$, simulating the direct hit scenario which is given by de Mink et al. (2013) as

$$\dot{J}_{\rm mt} = -\dot{M}_{1R}(1.7GM_2R_{\rm min})^{1/2}. \quad (18)$$

The change in the accreting star's spin angular momentum due to tidal interaction is expressed as

$$\dot{J}_{\rm tide} = -3M_2R_2^2(\Omega_2 - \omega_{\rm orb})\left(\frac{GM_2}{R_2^3}\right)^{1/2}\left[q^2\left(\frac{R_2}{a}\right)^6\right]E_2S_{22}^{5/3}, \quad (19)$$

where the quantity I_2 is the moment of inertia of the star 2, $\omega_{\rm orb}$ is the orbital angular velocity and is $(\frac{G(M_1+M_2)}{a^3})^{1/2}$, s_{22} is tidal frequency and is defined as $s_{22} = 2(\Omega_2 - \omega_{\rm orb})(\frac{R}{GM})^{1/2}$, and E_2 is a second-order tidal coefficient which depends on the stellar structure (Zahn 1975). It is expressed by $E_2 \sim 10^{-1.37}(\frac{R_{\rm conv,2}}{R_2})^8$ (Yoon et al. 2010). The quantity $R_{\rm conv,2}$ is the convective-core radius. Tidal interactions spin the star down when $\Omega_2 > \Omega_{\rm orb}$ and up $\Omega_2 < \Omega_{\rm orb}$ (Song et al. 2013, 2016). The tidal torque in the star with a convective envelop is given by

$$\dot{J}_{\rm tide} = -\omega_{\rm orb}6\frac{\lambda_{22}}{t_f}q^2M_2R_2^2\left(\frac{R_2}{a}\right)^6, \quad (20)$$

where the friction time is $t_f = (\frac{M_2R_2^2}{L_2})^{1/3}$, the quantity λ_{22} is same as that in Zahn (1989). In Eq. (17), the loss of the spin angular momentum through stellar winds is given by

$$\dot{J}_{\rm wind} = \frac{2}{3}\dot{M}_w\left(\frac{1}{1-\frac{v_2}{v_{\rm crit}}}\right)^\xi\Omega_2R_2^2, \quad (21)$$

where we take $\xi = 0.43$, $\dot{M}_w$ to be the mass-loss rate by stellar winds and it is given by de Jager et al. (1988). We have adopted the enhanced mass-loss rate of Langer (1998).

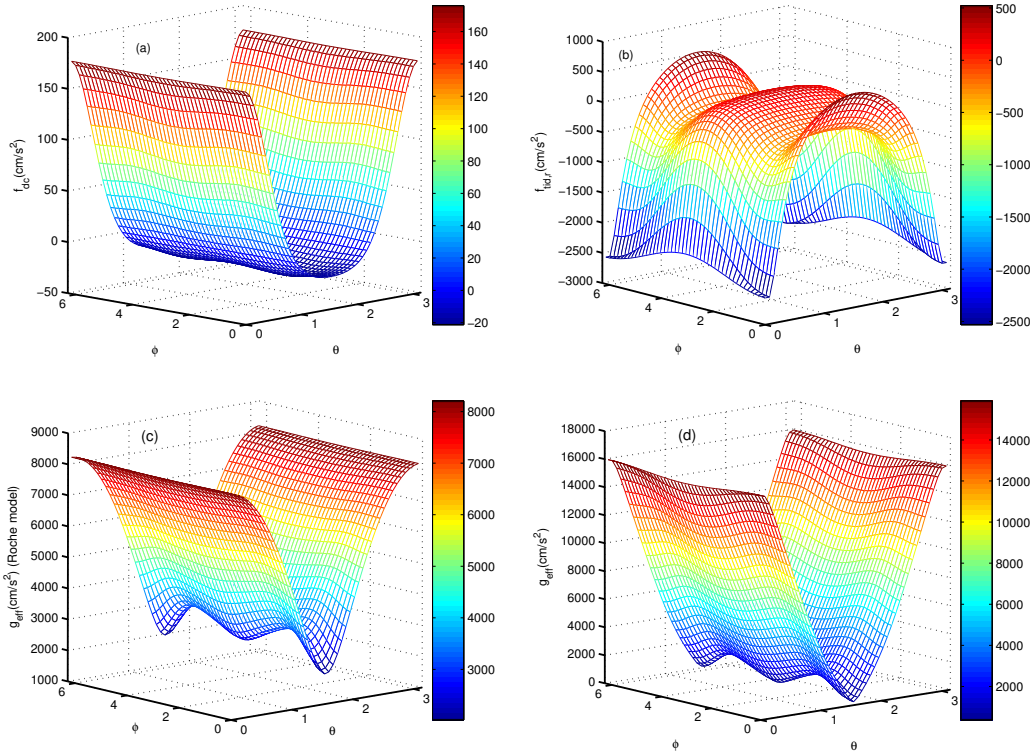

Fig. 2. Panel **a)**: variation of the force $\boldsymbol{f}_{\rm dis,rot}$ which is derived form the potential function $\Psi_{\rm dis,rot}$ versus coordinates θ and φ at the surface of accretors in model M1. Panel **b)**: variation of the radial component of tidal forces which is derived from the potential function $\Psi_{\rm tide}$ at the surface of accretor versus coordinates θ and φ in model M1. Panel **c)**: variation of the gravitational acceleration $|g_{\rm eff}|$ at the secondary star's surface under coordinates θ and φ in Roche model. The radius is treated as the constant value. Panel **d)**: variation of the gravitational acceleration $|g_{\rm eff}|$ at the secondary star's surface under coordinates θ and φ in model M1. The effective gravitational acceleration can be derived from Eq. (1).

4. Results of numerical calculation

4.1. The depiction of models

We used the most recent stellar evolution code TWIN, originally written by Eggleton (1971, 1972, 1973) and Eggleton et al. (1973). The nuclear reaction rates were from Caughlan & Fowler (1988) and were updated by Pols et al. (1995) and Stancliffe et al. (2005). The procedures used have been more recently updated by Han et al. (1994). The conservative binary-star evolution has been discussed by Nelson & Eggleton (2001). The convection is treated by mixing-length theory (Bohm-Vitense 1958) and a model for convective overshooting is included (Schroder et al. 1997). We have adopted the mass-loss rates of Vink et al. (2001) for massive stars. The two component stars in the binary system were calculated simultaneously. The initial mass of the system components was set at 20 $M_\odot$ and 16 $M_\odot$ with the metallicity of the Sun $X = 0.7$ and $Z = 0.02$. We took the mixing length parameter $\alpha = l/H_P$ to be 2.0. We note that in this study, we focus on the structure of the accreting star at the critical rotation. We have calculated two different types of model. They are as follows:

- MKE: the configurations of the two components are assumed to be spherical. In this case, $f_p = 1 - \frac{2\Omega^2 r^3}{3GM_\psi}$, $f_t = 1$, the effect of rotation on stellar structure is only taken into account as a reduction of the effective gravity. This method is referred to as the KE method (Kähler 1986). Moreover, rotational mixing has been included in this model. The initial spin periods $P_{\rm s,1,2}$ for two components are taken the values of 1.5 days while the initial orbital period is 2.65 days.
- M1: the effect of distortions and mixing processes have been included. The accreting star can be spun up during rapid mass transfer. The initial spin periods $P_{\rm s,1,2}$ for two components and the initial orbital period are the same as the ones in model MKE.

4.2. Impact of the structure of the rotating star

4.2.1. The distribution of the force derived from the quadrupolar potential $\Psi_{\rm dis,rot}$

In order to investigate the structure of the critically rotating accretor, we have chosen the evolutionary time of $t = 6.3323$ Myr. The velocity of the secondary star reaches $\sim 0.95 v_{\rm cri,1}$ due to rapid mass transfer in model M1, and the spin period is 0.729 d. The orbital period is 2.315 d and the mass of the secondary star is 16.153 $M_\odot$. The mass of the primary star is 19.481 $M_\odot$.

Panel a in Fig. 2 shows the variations of the force $\boldsymbol{f}_{\rm dis,rot}$ ($\boldsymbol{f}_{\rm dis,rot} = -\frac{\partial \Psi_{\rm dis,rot}}{\partial r}$) which are derived from the rotational distortion potential $\Psi_{\rm dis,rot}$. The positive value indicates that the force pulls the accretor outward (away from the accretor) whereas the negative value denotes that the force pushes the accretor inward. This force arrives at 1.776×10^2 cm/s^2 at two polar points E and F (cf. Fig. 1). It goes down to -18.116 cm/s^2 and contributes -3.02% to the radial centrifugal force at the point A. The primary minimum has a value of -22.790 cm/s^2 at points B and D and dominates a fraction of about -4.14% for the radial centrifugal force. The secondary minimum is -19.438 cm/s^2 at the position of point C and contributes -3.39% to the radial centrifugal force. The result implies that the force $\boldsymbol{f}_{\rm dis,rot}$ can lead to a reduction of the self gravity ($\frac{GM_2}{R_2}$) at the two poles, and a increase of the gravity at the equator.

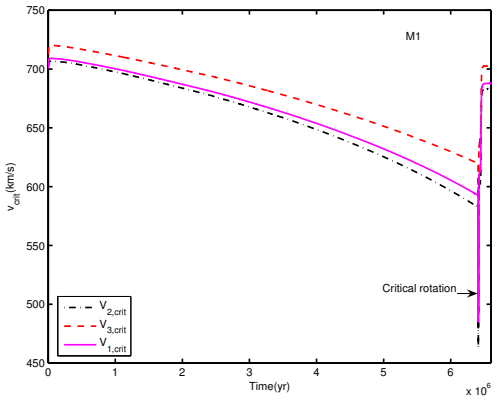

Fig. 3. Time evolution of the critical velocities for three models. The critical velocity $v_{1,\rm crit}$ is derived from the total potential function $\Psi = \Psi_{\rm grav}+\Psi_{\rm rot}+\Psi_{\rm tide}+\Psi_{\rm dis,rot}+\Psi_{\rm dis,tide}$ in model M1(Solid line). The critical velocity $v_{2,\rm crit}$ is derived from potential function $\Psi = \Psi_{\rm grav}+\Psi_{\rm rot}+\Psi_{\rm tide}$ in model M1 (Dot-dashed line). The critical velocity $v_{3,\rm crit}$ is derived from the potential function $\Psi_r = \Psi_{\rm grav}+\Psi_{\rm rot}+\Psi_{\rm dis,rot}$ in model M1 (Dashed line).

The force $\boldsymbol{f}_{\rm dis,rot}$ can significantly affect the critical velocity and oblateness (cf. Fig. 3) of accretors. The quadrupolar correction due to tides $\Psi_{\rm dis,tide}$ is smaller by a factor of ten than the one of rotational distortion $\Psi_{\rm dis,rot}$. Therefore, it may be neglected because of long orbital period of 2.315 d.

4.2.2. The distribution of tidal forces

Panel b shows variations of the radial component of the tidal force which is derived from $\Psi_t = \Psi_{\rm tide}+\Psi_{\rm dis,tide}$ at the surface of the secondary star under coordinate θ and φ in the model M1. It is shown that the radial component of tidal forces goes up from -2.555×10^3 cm/s^2 at two polar points to 5.466×10^2 cm/s^2 at the point A. The tidal force can reach 2.59787×10^2 cm/s^2 at the point C. The difference in the tidal force between points A and C comes from the term $\psi_{\rm tide}$ ($j=3$) in Eq. (1) which counteracts the self gravity. Tidal forces greatly shorten the polar radius of accretors, causing the polar radius to become smaller than the equatorial radius. Tides and centrifugal forces pull the accretor outwards at points A and C and cause the equatorial radii to increase. The equatorial radius $r_{\rm e1}$ which confronts the companion star is the biggest one because the tidal force which originates form the term $\psi_{\rm tide}$ ($j=3$) at point A can strengthen the centrifugal force. The radial component of tidal forces has a value of -2.144×10^2 cm/s^2 at the points B and D. For close binaries, the symmetry around the rotation axis is broken by tidal forces and this might produce additional possibilities for internal mixing due to thermal inequalities in the equatorial circle.

These facts show that tidal forces can produce an increase in the effective gravitational acceleration at the two poles. The opposite effect is located at points A and C. At points B and D, tidal forces counteracts with the centrifugal force, leading to a increase in self gravities. Therefore, the shortest equatorial radius is $r_{\rm e3}$.

The critical oblateness (the ratio of the equatorial radius to the polar one) can be increased when the quadrupolar moment is taken into account. The reason is that if $\psi_{\rm dis,rot}$ is increased, a test particle at equator will experience a stronger self gravity. The star needs to attain a high spin angular velocity and the new location of test particles is situated closer to the companion star to re-establish a zero-acceleration. At critical rotation, a maximum oblateness can attain a value of $\frac{r_{\rm e}}{r_p}=1.5$ according to Roche model. Zahn (2010) shows that the critical flattening can attain $\frac{r_{\rm e1}}{r_p}=1.5+2.1k_2\simeq1.502-1.521$ in single rotating star when the quadrupolar moment has been included. The quantity k_2 is given by $k_2=\frac{3-\eta_2(R_2)}{2(2+\eta_2(R_2))}$ and is typically of the order of $10^{-3}-10^{-2}$ for main-sequence stars. In our binary model, the critical flattening $\frac{r_{\rm e1}}{r_p}$ can be approximately estimated by the value of $\frac{r_{\rm e1}}{r_p}=(1.5+2.1k_2)(1+\frac{B(r_0)}{2})\simeq1.5469$ at this evolutionary point. Due to tide forces, the critical flattening can exceed the value in the model of single rotating star, produced by Zahn's model. Furthermore, we find that the critical flattening generally decreases in time due to the star's nuclear evolution. The reason is that the value of k_2 generally decreases in time due to the increasing of the mean molecular weight in the stellar core.

4.2.3. Comparing the effective gravities derived from Roche model and distorted model

The surface gravity $|g_{\rm eff}|$ for the accretor M_2 which is derived from Roche model in Eq. (A.35) is shown in panel c. The effective gravity $|g_{\rm eff}|$, derived from Eq. (1) is illustrated in panel d. Comparing panel c with d, we find that the effective gravity increases ~48.6% at the two polar points and decreases by ~87.5% at point A for the distorted model. The surface effective gravity can decrease by a factor of ~49.3% at points B and point D. Therefore, the effective gravity has a smaller value at the equator and a higher value at two polar points in distorted models. The main reason for this is that the distribution of the effective gravity depends strongly on the distance between the stellar center and the surface. The deformed model treats the star as the triaxial ellipsoid with different radii, whereas the Roche model treats the stellar surface as a sphere.

4.3. The critical velocity

The time evolution of the critical velocity for three models is displayed in Fig. 3. Comparing $v_{2,\rm crit}$ with $v_{3,\rm crit}$, we find that tidal forces reduce the critical velocity. The reason for this is that tidal forces can offset the gravity at the points confronting the companion (i.e. at point A). Compared $v_{2,\rm crit}$ with $v_{1,\rm crit}$, we find that distortions induced by rotation and tide can enhance the critical velocity. This can be understood as the force which is derived from $\psi_{\rm dis,rot}$ can help the self gravity to offset the centrifugal force at the point facing towards the companion.

4.4. Two rotational factors f_p and f_t

Figure 4 shows two correction factors f_p and f_t as a function of the dimensionless radius $R/R_\odot$ according to the MKE model and to the present method with model M1. We see that f_p declines from 1.0 to 0.652 in the MKE model whereas it declines from 1.0 to 0.363 in present method. The factor f_p in model M1 is same as that in the MKE model in the central region because stellar core has a high density. We suggest that the MKE model should be applied only to the inner layers where the local density is greater than the mean density.

Compared MKE model with M1, we find that the maximum correction for the factor f_p can attain 44.3% at the stellar surface. The result implies that the surface effective gravity $\langle g_{\rm e}\rangle$ in model M1 has a lower value in distorted model than the one in MKE. The main reason is that great distortions can enhance the centrifugal force. The contribution of this effect to the effective gravity can reach the first order effect ~20% (cf. Fig. 4) and can not be neglected. Distortions induced by rotation and tides

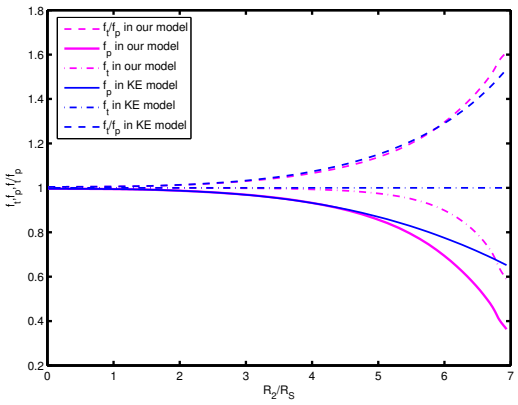

Fig. 4. Correction factors f_p, f_t, and, f_t/f_p versus the dimensionless radius $R/R_\odot$ according to model MKE (blue curve) and to model M1 (pink curves).

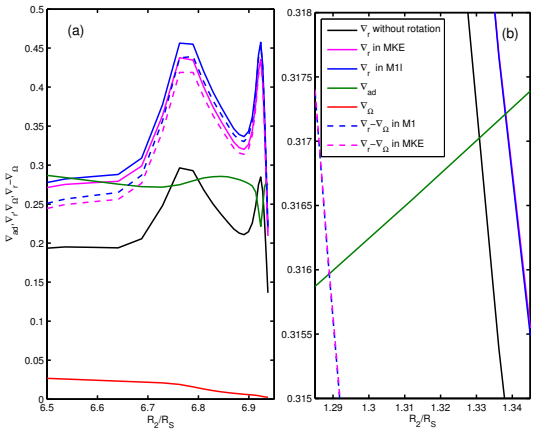

Fig. 5. *Left panel*: temperature gradients ∇_r, $\nabla_{\rm ad}$, and $\nabla_r - \nabla_\Omega$ as function of the dimensionless radius $R/R_\odot$ according to the MKE model (blue curves) and the M1 model (pink curves) below the stellar surface. The black line denotes the radiative temperature gradient ∇_r in the model without rotation. The green line denotes the temperature gradients $\nabla_{\rm ad}$. The red curve indicates the quantity ∇_Ω. *Right panel*: various temperature gradients located at the border of the convective core. The point where black lines cut green lines implies the border of convective core in non-rotating model according to the Schwarzschild criterion. The point where blue lines cut green lines indicates the border of convective core in rotating model according to the Schwarzschild criterion.

can contribute a significant fractional importance to the effective gravity in the outer stellar layers.

The small factor f_p in model M1 implies that the accreting star will have a bigger radius and that matter may be evaded easily on the surface. Moreover, the lower factor f_p can cause the star to shift dramatically towards low temperature and low luminosity due to gravity darkening. The dynamical timescale may be extended because of larger effective radii and cooler surface temperatures. It is more difficult for a rapidly rotating star to attain hydrostatic equilibrium.

Also, we can see that f_t keeps a constant value of 1.0 through the whole star in the MKE method whereas it reduces from 1.0 to 0.585 in the present method. It is illustrated that the maximum correction for the factor f_t reaches 41.5% at the stellar surface. The ratio of f_t to f_p in the MKE model is smaller than the one in M1 below stellar surface.

4.5. The expansion of convective zones

It is shown in panel a of Fig. 5 that various temperature gradients are functions of the dimensionless radius $R_2/R_\odot$. Without rotation, there is a thin outer convective zone which is close to the stellar surface. It extends from 6.74 $R_\odot$ to 6.80$R_\odot$ – only 0.86% of the radius – and contains a very small fraction of the total stellar mass ($\sim 5.0 \times 10^{-7}$). With a ratio $\frac{\Omega}{\Omega_{\rm crit}} = 0.95$ in model M1, convective zones of rapid rotating accretors extend according to Solberg-Hoiland criterion. The outer convective zones extend from 6.641 $R_\odot$ to 6.937 $R_\odot$ in model MKE whereas they extend from 6.590 $R_\odot$ to 6.937 $R_\odot$ in the distorted model M1. The outer convective layer is deeper in model M1 than the one in model MKE. The reason is that the quantity $\frac{f_t}{f_p}$ in model M1 has a high value in the outer envelope. Therefore, great deformations that are induced by rotation and tides are in favor of convective motion.

It is shown in panel b that rapidly rotating accretors have a bigger convective core of $\sim$1.338 $R_\odot$ according to the Schwarzschild criterion compared with the non-rotational model with a convective core of 1.331 $R_\odot$. If the Solberg-Hoiland criterion for stability is adopted, rotating accretors will have a small convective core of 1.29 $R_\odot$. Therefore, the Solberg-Hoiland criterion tends to reduce the central convective region and contribute to a low stellar luminosity.

4.6. The energy generation and hydrogen profiles

Variations of the energy generation by nuclear reactions as a function of the Lagrangian mass at four different evolutionary points are shown in left panel of Fig. 6. We find that the region and the intensity of the energy generation through nuclear reactions decrease with the evolution. The reason for this is that centrifugal forces compensate most of the gravity; pressure and temperature in the central parts of accretor are smaller, consequently the energy production rate is also decreasing. (cf. panel b in Fig. 6).

Internal distribution of hydrogen mass fraction of the Lagrangian mass in the model M1 is shown in right panel of Fig. 6. There is a distinct boundary between the convective core and the radiative envelope before mass transfer (at the time of t = 3.5458 Myr). At the time of $\sim$6.320 Myr, the accreting star approaches the critical rotation due to RLOF. From then on, the gradient of internal distribution of hydrogen become smaller and smaller. The reason fo this is that the amplitude of the radial component of the meridional velocity U which scales with Ω is the main driving mechanism for mixing of chemical elements. The result implies that rotationally induced chemical mixing is more efficient and occurs faster than the build-up of chemical gradients at the cutting edge of nuclear fusion (Maeder 1987). Moreover, more massive fuel hydrogen is transported from the outer envelope to the core and these physical processes may prolong the time the accretor spends on the main sequence.

5. Conclusions and summary

The configuration of accretors is one of triaxial ellipsoids which are deformed by tides. The symmetry around the rotation axis is broken by tides and this might produce additional possibilities for internal processes to enhance mixing due to thermal inequalities in the equatorial circle.

The self gravity is balanced by the combined effect of centrifugal forces, rotational distortions, and tidal forces at equator. Therefore, the critical velocity is reduced due to tidal force. The force which is derived from the potential $\Psi_{\rm dis,rot}$ can help the self gravity to offset the centrifugal force at the equator. We can derive a higher critical velocity from the distorted model which includes rotational distortion $\Psi_{\rm dis,rot}$.

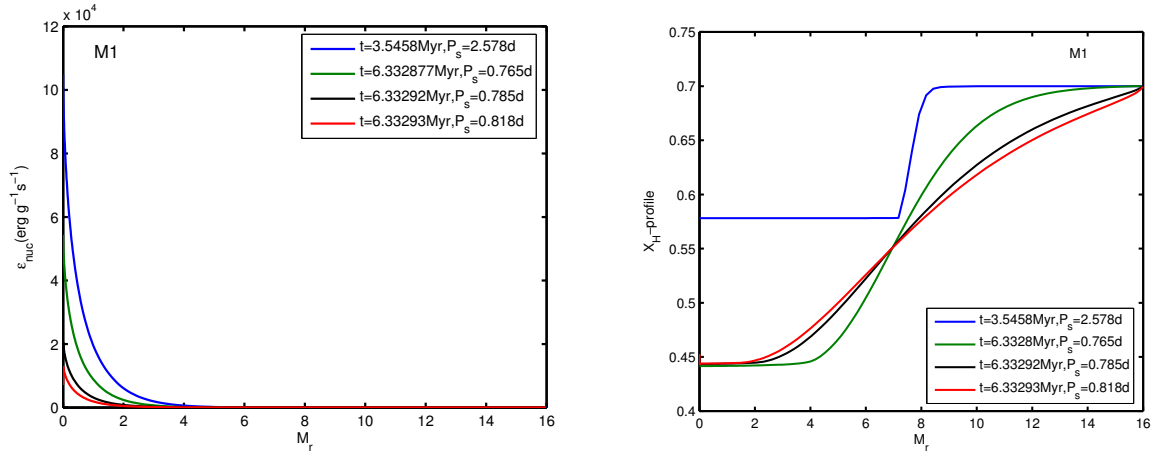

Fig. 6. *Left panel*: variations of the energy generation by nuclear reactions as a function of the Lagrangian mass at four different evolution points at critical rotation. The recipient approaches the critical rotation at the time of ~6.33 Myr. *Right panel*: variation of internal distribution of hydrogen mass fraction as a function of the Lagrangian mass at four different evolution points.

The mean effective gravity $\langle g_e \rangle$ can be reduced dramatically in the distorted model due to a small factor f_p. The ratio of f_t to f_p is bigger in model M1 than that in the MKE model. The star appears a deeper convective zone below stellar surface. The accreting star has a bigger convective core according to the Schwarzschild criterion but it will allow a smaller convective core according to the Solberg-Hoiland criterion.

The critical flattening (defined as the ratio between the equatorial and polar radii) can be increased to 1.5469 and exceed the 1.5 value of Roche model as a result of considering the quadrupolar moment and tidal forces.

The gradient of hydrogen profile becomes smaller and smaller due to rapid meridional circulation and the accretor is mixed efficiently. Both the rate of energy generations and convective core decrease due to the lower temperature produced by the combined effect of rotation and tide. The lifetime of the accreting star during the main sequence can be extended due to efficient mixing and lower rate of energy generations.

Acknowledgements. We thank an anonymous referee. Also, we are very grateful to Professor Peter P. Eggleton for sharing his binary evolution code. This work was sponsored by the National Natural Science Foundation of China (Grant Nos. 11463002 and 11373020), the Open Foundation of key Laboratory for the Structure and evolution of Celestial Objects, Chinese Academy of Science (Grant Nos. OP201405, OP201404(B615015)), the Science Foundation of Jimei University (Grant No. C613030), and Science and Technology Foundation of Guizhou Province (Grant LKK[2013] No. 20).

References

Bohm-Vitense, E. 1958, Z. Astrophys., 46, 108
Caughlan, G. R., & Fowler, W. A. 1988, Atomic Data and Nuclear Data Tables, 40, 283
Decressin, T., Mathis, S., Palacios, A., et al. 2009, A&A, 495, 271
de Jager, C., Nieuwenhuijzen, H., & van der Hucht, K. A. 1988, A&AS, 72, 259
de Mink, S. E., Langer, N., Izzard R. G., Sana, H. & Koter A. D. 2013, ApJ, 764, 166
Eggleton, P. P. 1971, MNRAS, 151, 351
Eggleton, P. P. 1972, MNRAS, 156, 361
Eggleton, P. P. 1973, MNRAS, 163, 279
Eggleton, P. P. 1983, ApJ, 268, 368
Eggleton, P. P., & Kiseleva, L. 1998, ApJ, 499, 853
Eggleton, P. P., Faulkner, J., & Flannery, B. P. 1973, A&A, 23, 325
Endal, A. S., & Sofia, S. 1976, ApJ, 210, 184
Endal, A. S., & Sofia, S. 1978, ApJ, 220, 279
Georgy, C., Meynet, G., Maeder, A., et al. 2011, A&A, 527, A52
Han, Z., Podsiadlowski, P., & Eggleton, P. P. 1994, MNRAS, 270, 121
Heger, A., Langer, N., & Woosley, S. E. 2000, ApJ, 528, 368
Huang, R. Q. 2004, A&A, 422, 981
Huang, R. Q., & Taam, R. E. 1990, A&A, 236, 107
Kähler, H. 1986, A&A, 157, 329
Kippenhahn, R., & Thomas, H. C. 1970, Stellar Rotation, ed. A. Slettebak (Gordon and Breach Science Publishers), Proc. IAU Colloq., 4, 20
Kippenhahn, R., & Weigert, A. 1990, Stellar Structure and Evolution (Berlin, Heidelberg, New York: Springer-Verlag), Astron. Astrophys. Lib., 468
Kopal, Z. 1959, Close Binary Systems (London, UK: Chapman & Hall)
Kopal, Z. 1960, Figures of Equilibrium of celestial bodies (The University of Wisconsin Press)
Kopal, Z. 1974, Ap&SS, 27, 389
Landin, N. R., Mendes, L. T. S., & Vaz, L. P. R. 2009, A&A, 494, 209
Langer, N. 1998, A&A, 329, 551
Langer, N. 2012, ARA&A, 50, 107
Langer, N., Wellstein, S., & Petrovic, J. 2003, A Massive Star Odyssey: From Main Sequence to Supernova, Proc. IAU Symp., 212, 275
Mathis, S., & Zahn, J.-P. 2004, A&A, 425, 229
Mathis, S., Palacios, A., & Zahn, J.-P. 2004, A&A, 425, 243
Maeder, A. 2003, A&A, 399, 263
Maeder, A., & Meynet, G. 2000, ARA&A, 38, 143M
Maeder, A., & Meynet, G. 2012, Rev. Mod. Phys., 84, 25
Maeder, A., & Zahn, J. -P. 1998, A&A, 334, 1000
Maeder, A., Georgy, C., & Meynet, G. 2008, A&A, 479, L37
Meynet, G., & Maeder, A. 2000, A&A, 361, 101
Meynet, G., Ekström, S., & Maeder, A. 2006, A&A, 447, A623
Meynet, G., Hirschi, R., Ekstrom, S., et al. 2010, A&A, 521, A30
Nelson, C. A., & Eggleton, P. P. 2001, ApJ, 552, 664
Packet, W. 1981, A&A, 102, 17
Pinsonneault, M. H., Kawaler, S. D., Sofia, S., & Demarque, P. 1989, ApJ, 338, 424
Pols, O. R., Tout, C. A., Eggleton, P. P., & Han, Z., 1995, MNRAS, 274, 964
Press, W. H., Teukolsky, S. A., Vetterling, W. T., & Flannery, B. P. 1992, Numerical Recipes in Fortran 77: The art of Scientific Computing (Cambridge University Press)
Rieutord, M. 2006, A&A, 451, 1025
Schroder, K. P., Pols, O. R. & Eggleton, P. P. 1997, MNRAS, 285, 696
Song, H. F., Zhong, Z., & Lu, Y. 2009, A&A, 504,161
Song, H. F., Lu, Y., & Wang, J. Z. 2011, PASJ, 63, 835
Song, H. F., Maeder, A., Meynet, G., et al. 2013, A&A, 556, A100
Song, H. F., Meynet, G., Maeder, A., Ekström, S., & Eggenberger, P. 2016, A&A, 585, A120
Stancliffe, R. J. 2005, Ph.D. Thesis, University of Cambridge
Talon, S., & Zahn, J.-P. 1997, A&A, 317, 749
Ulrich, R. K., & Burger, H. L. 1976, ApJ, 206, 509
Vink, J. S., de Koter, A., & Lamers, H. J. G. L. M. 2001, A&A, 369, 574
von Zeipel, H., 1924, MNRAS, 84, 665
Yoon, S. C., & Woosley, S. E., & Langer, N. 2010, ApJ, 725, 940
Zahn, J.-P. 1975, A&A, 41, 329
Zahn, J.-P. 1992, A&A, 265, 115
Zahn, J.-P., & Bouchet, L. 1989, A&A, 223, 112

Appendix A

A.1. The potential including rotational and tidal distortions and the gravitational acceleration

At the position $P(r,\theta,\varphi)$, the total potential for the combined effect of rotation and tide can be expressed in Cartesian spherical coordinate systems. It is given by (Landin et al. 2009; Song et al. 2009)

$$\Psi(r,\theta,\varphi) = \frac{GM_\psi}{r} + \frac{1}{2}\Omega_2^2 r^2\sin^2\theta + \frac{GM_1}{a}\left[1+\sum_{j=2}^{4}\left(\frac{r_0}{a}\right)^j P_j(\lambda)\right] - \frac{4\pi}{3r^3}P_2(\cos\theta)\int_0^{r_0}\rho\frac{r_0'^7}{M_\psi}\Omega_2^2\frac{5+\eta_2}{2+\eta_2}\mathrm{d}r_0' + 4\pi G M_2\sum_{j=2}^{4}\frac{P_j(\lambda)}{(ra)^{j+1}}\int_0^{r_0}\rho\frac{r_0'^{2j+3}}{M_\psi}\frac{j+3+\eta_j}{j+\eta_j}\mathrm{d}r_0'. \quad (A.1)$$

The equipotential surface of the distorted star can be described by (Landin et al. 2009)

$$r(r_0,\theta,\varphi) = r_0\left(1+Y_{\rm rot}+\sum_{j=2}^{4}Y_j\right), \quad (A.2)$$

where $Y_{\rm rot}$ is a measure of the deviation from sphericity caused by rotation and given by $Y_{\rm rot} = -\frac{\Omega_2^2 r_0^3}{3GM_\psi}\frac{5}{2+\eta_2(r_0)}P_2(\cos\theta)$. The quantity Y_j is a measure of the deviation from sphericity caused by the tide and given by $Y_j = \frac{M_1}{M_\psi}\frac{2j+1}{j+\eta_j(r_0)}(\frac{r_0}{R})^{j+1}P_j(\lambda)$. r_0 is the radius of the equipotential surface at the angles (θ_0,φ_0), defined such that

$$-A(r_0)P_2(\cos\theta_0) + B(r_0)P_2(\lambda_0) + C(r_0)P_3(\lambda_0), + D(r_0)P_4(\lambda_0) = 0 \quad (A.3)$$

where the quantities $A(r_0)$, $B(r_0)$, $C(r_0)$, and $D(r_0)$ are defined by

$$A(r_0) = \frac{\Omega_2^2 r_0^3}{3GM_{2\psi}}\frac{5}{2+\eta_2} \quad (A.4)$$
$$B(r_0) = \frac{M_1}{M_{2\psi}}\left(\frac{r_0}{a}\right)^3\frac{5}{2+\eta_2}$$
$$C(r_0) = \frac{M_1}{M_{2\psi}}\left(\frac{r_0}{a}\right)^4\frac{7}{3+\eta_3}$$
$$D(r_0) = \frac{M_1}{M_{2\psi}}\left(\frac{r_0}{a}\right)^5\frac{9}{4+\eta_4}.$$

The equipotential surface of the stars can be described as

$$r(r_0,\theta,\varphi) = r_0[1 - A(r_0)P_2(\cos\theta) + B(r_0)P_2(\lambda) + C(r_0)P_3(\lambda) + D(r_0)P_4(\lambda)]. \quad (A.5)$$

By integrating Eq. (26) from 0 to $r(r_0,\theta,\varphi)$, we obtain that the volume V_ψ of the topologically equivalent sphere with the radius r_ψ,

$$r_\psi = r_0\left[1+\frac{3A^2}{5}+\frac{3AB}{5}+\frac{3B^2}{5}+\frac{3C^2}{7}-\frac{2A^3}{35}-\frac{3A^2B}{35} + \frac{9A^2D}{140}+\frac{3AB^2}{35}+\frac{2AC^2}{35}+\frac{2B^3}{35}\frac{10AD^2}{231}+\frac{6ABD}{35} + \frac{6B^2D}{35}+\frac{4BC^2}{35}+\frac{6C^2D}{77}+\frac{20BD^2}{231}+\frac{18D^3}{1001}+\frac{D^2}{3}\right]^{\frac{1}{3}}. \quad (A.6)$$

Differenting the potential function, we can derive three components of the effective gravitational acceleration g_r, g_θ, and, g_φ. They are

$$g_r(r,\theta,\varphi) = -\frac{\partial\Psi}{\partial r} = \frac{GM_\psi}{r^2} - \Omega_2^2 r\sin^2\theta - \sum_{j=2}^{4}\frac{GM_1}{a^{j+1}}jr_0^{j-1}P_j(\lambda)\frac{\mathrm{d}r_0}{\mathrm{d}r} - \frac{4\pi}{r^4}P_2(\cos\theta)\int_0^{r_0}\rho\frac{r_0'^7}{M_\psi}\Omega_2^2\frac{5+\eta_2}{2+\eta_2}\mathrm{d}r_0' + \frac{4\pi}{3r^3}P_2(\cos\theta)\rho\frac{r_0'^7}{M_\psi}\Omega_2^2\frac{5+\eta_2}{2+\eta_2}\frac{\mathrm{d}r_0}{\mathrm{d}r} + 4\pi GM_1\sum_{j=2}^{4}(j+1)\frac{P_j(\lambda)}{a^{j+1}}\frac{1}{r^{j+2}}\int_0^{r_0}\rho\frac{r_0'^{2j+3}}{M_\psi}\frac{j+3+\eta_j}{j+\eta_j}\mathrm{d}r_0' - 4\pi GM_1\sum_{j=2}^{4}\frac{P_j(\lambda)}{(ra)^{j+2}}\rho\frac{r_0^{2j+3}}{M_\psi}\frac{j+3+\eta_j}{j+\eta_j}\frac{\mathrm{d}r_0}{\mathrm{d}r}, \quad (A.7)$$

$$g_\theta(r,\theta,\varphi) = -\frac{1}{r}\frac{\partial\Psi}{\partial\theta} = -\Omega_2^2 r\sin\theta\cos\theta - \frac{GM_1}{a^3r}r_0^2P_2'(\lambda)_\theta - \frac{GM_1}{a^4r}r_0^3P_3'(\lambda)_\theta - \frac{GM_1}{a^5r}r_0^4P_4'(\lambda)_\theta - \frac{GM_1}{r}\sum_{j=2}^{4}jr_0^{j-1}\frac{1}{a^{j+1}}P_j(\lambda)\frac{\mathrm{d}r_0}{\mathrm{d}\theta} + \frac{4\pi}{3r^4}P_2'(\lambda)_\theta\int_0^{r_0}\rho\frac{r_0'^7}{M_\psi}\Omega_2^2\frac{5+\eta_2}{2+\eta_2}\mathrm{d}r_0' + \frac{4\pi}{3r^4}P_2(\theta)\rho\frac{r_0^7}{M_\psi}\Omega_2^2\frac{5+\eta_2}{2+\eta_2}\frac{\mathrm{d}r_0}{\mathrm{d}\theta} - \frac{4\pi GM_1}{r}\sum_{j=2}^{4}\frac{P_j(\lambda)}{(ra)^{j+1}}\rho\frac{r_0^{2j+3}}{M_\psi}\frac{j+3+\eta_j}{j+\eta_j}\frac{\mathrm{d}r_0}{\mathrm{d}\theta} - \frac{4\pi GM_1}{r^4a^3}P_2'(\lambda)_\theta\int_0^{r_0}\rho\frac{r_0'^7}{M_\psi}\frac{5+\eta_2}{2+\eta_2}\mathrm{d}r_0' - \frac{4\pi GM_1}{r^5a^4}P_2'(\lambda)_\theta\int_0^{r_0}\rho\frac{r_0'^9}{M_\psi}\frac{6+\eta_3}{3+\eta_3}\mathrm{d}r_0' - \frac{4\pi GM_1}{r^6a^5}P_4'(\lambda)_\theta\int_0^{r_0}\rho\frac{r_0'^{11}}{M_\psi}\frac{7+\eta_4}{4+\eta_4}\mathrm{d}r_0' \quad (A.8)$$

$$g_\varphi(r,\theta,\varphi) = -\frac{1}{r\sin\theta}\frac{\partial\Psi}{\partial\varphi} = -\frac{GM_1}{r\sin\theta}\sum_{j=2}^{4}\frac{jr_0^{j-1}}{a^{j+1}}P_j(\lambda)\frac{\mathrm{d}r_0}{d\varphi} - \frac{GM_1r_0^2}{r\sin\theta a^3}P_2'(\lambda)_\varphi - \frac{GM_1r_0^3}{r\sin\theta a^4}P_3'(\lambda)_\varphi + \frac{GM_1r_0^4}{r\sin\theta a^5}P_4'(\lambda)_\varphi + \frac{4\pi}{3r^4\sin\theta}P_2(\cos\theta)\rho\frac{r_0^7}{M_\psi}\Omega_2^2\frac{5+\eta_2}{2+\eta_2}\frac{\mathrm{d}r_0}{d\varphi} - \frac{4\pi GM_1}{r\sin\theta}\frac{1}{(ra)^3}P_2'(\lambda)_\varphi\int_0^{r_0}\rho\frac{r_0'^7}{M_\psi}\frac{5+\eta_2}{2+\eta_2}\mathrm{d}r_0' - \frac{4\pi GM_1}{r\sin\theta}\frac{1}{(ra)^4}P_3'(\lambda)_\varphi\int_0^{r_0}\rho\frac{r_0'^9}{M_\psi}\frac{6+\eta_3}{3+\eta_3}\mathrm{d}r_0' - \frac{4\pi GM_1}{r\sin\theta}\frac{1}{(ra)^5}P_4'(\lambda)_\varphi\int_0^{r_0}\rho\frac{r_0'^{11}}{M_\psi}\frac{7+\eta_4}{4+\eta_4}\mathrm{d}r_0' + \frac{4\pi GM_1}{r\sin\theta}\sum_{j=2}^{4}\frac{P_j(\lambda)}{(ra)^{j+1}}\rho\frac{r_0^{2j+3}}{M_\psi}\frac{j+3+\eta_j}{j+\eta_j}\frac{\mathrm{d}r_0}{d\varphi}, \quad (A.9)$$

where

$$\frac{\mathrm{d}r_0}{\mathrm{d}r} = \frac{1}{g_1(r_0,\theta,\varphi)}, \tag{A.10}$$

$$\frac{\mathrm{d}r_0}{\mathrm{d}\theta} = \frac{g_2(r_0,\theta,\varphi)}{g_1(r_0,\theta,\varphi)}, \tag{A.11}$$

$$\frac{\mathrm{d}r_0}{d\varphi} = \frac{g_3(r_0,\theta,\varphi)}{g_1(r_0,\theta,\varphi)}, \tag{A.12}$$

$$g_1(r_0,\theta,\varphi) = 1 - 4A(r_0)P_2(\cos\theta) + 4B(r_0)P_2(\lambda) + 5C(r_0)P_3(\lambda) + 6D(r_0)P_4(\lambda), \tag{A.13}$$

$$g_2(r_0,\theta,\varphi) = -r_0\Big[\frac{3}{2}A(r_0)\sin 2\theta + \frac{3}{2}B(r_0)\sin 2\theta\cos^2\varphi + \frac{1}{2}C(r_0)(15\sin^2\theta\cos\theta\cos^3\varphi - 3\cos\theta\cos\varphi) + \frac{1}{8}D(r_0)(140\sin^3\theta\cos\theta\cos^4\varphi - 30\sin 2\theta\cos^2\varphi)\Big] \tag{A.14}$$

$$g_3(r_0,\theta,\varphi) = r_0\Big[\frac{3}{2}B(r_0)\sin^2\theta\sin 2\varphi + \frac{1}{2}C(r_0)(15\sin^3\theta\cos^2\varphi\sin\varphi - 3\sin\theta\sin\varphi) + \frac{1}{8}D(r_0)(140\sin^4\theta\cos^3\varphi\sin\varphi - 60\sin^2\theta\sin 2\varphi)\Big], \tag{A.15}$$

where

$$P_2'(\cos\theta)_\theta = -3\cos\theta\sin\theta, \tag{A.16}$$

$$P_2'(\sin\theta\cos\varphi)_\theta = 3\sin\theta\cos\theta\cos^2\varphi, \tag{A.17}$$

$$P_3'(\sin\theta\cos\varphi)_\theta = \frac{1}{2}(15\sin^2\theta\cos\theta\cos^3\varphi - 3\cos\theta\cos\varphi), \tag{A.18}$$

$$P_4'(\sin\theta\cos\varphi)_\theta = \frac{1}{2}(35\sin^3\theta\cos\theta\cos^4\varphi - 15\sin^2\theta\cos\varphi\sin^2\varphi), \tag{A.19}$$

$$P_2'(\cos\theta)_\varphi = 0, \tag{A.20}$$

$$P_2'(\sin\theta\cos\varphi)_\varphi = -3\sin^2\theta\cos\varphi\sin\varphi, \tag{A.21}$$

$$P_3'(\sin\theta\cos\varphi)_\varphi = -\frac{1}{2}(15\sin^3\theta\cos^2\varphi\sin\varphi - 3\sin\theta\sin\varphi), \tag{A.22}$$

$$P_4'(\sin\theta\cos\varphi)_\varphi = -\frac{1}{2}(35\sin^4\theta\cos^3\varphi\sin\varphi - 15\sin^2\theta\sin\varphi\cos\varphi), \tag{A.23}$$

The local effective gravity is written as

$$g(r,\theta,\varphi) = \left[\left(\frac{\partial\Psi}{\partial r}\right)^2 + \left(\frac{1}{r}\frac{\partial\Psi}{\partial\theta}\right)^2 + \left(\frac{1}{r\sin\theta}\frac{\partial\Psi}{\partial\varphi}\right)^2\right]^{\frac{1}{2}}. \tag{A.24}$$

A.2. The expression of the surface element dσ on an equipotential of a rotating star

On the surface of the distorted star, the normal to the surface does not coincide with the direction of the vector radius. There is an angle ε between the directions of $\boldsymbol{r}$ and of $-\boldsymbol{g}_{\rm eff}$,

$$\cos\varepsilon = -\frac{\boldsymbol{g}_{\rm eff}\cdot\boldsymbol{r}}{|\boldsymbol{g}_{\rm eff}|\cdot|\boldsymbol{r}|}, \tag{A.25}$$

Therefore, the surface element dσ can be expressed as

$$\mathrm{d}\sigma = \frac{r^2\sin\theta\mathrm{d}\theta\mathrm{d}\varphi}{\cos\varepsilon} = r\sin\theta(r^2 + \left(\frac{\partial r_0}{\partial\theta}/\frac{\partial r_0}{\partial r}\right)^2 + \frac{1}{\sin^2\theta}\left(\frac{\partial r_0}{\partial\varphi}/\frac{\partial r_0}{\partial r})^2\right)^{\frac{1}{2}}\mathrm{d}\theta\mathrm{d}\varphi = r\sin\theta r_0(f_1^2(r_0,\theta,\varphi) + f_2^2(r_0,\theta,\varphi) + f_3^2(r_0,\theta,\varphi))^{\frac{1}{2}}\mathrm{d}\theta\mathrm{d}\varphi, \tag{A.26}$$

where

$$f_1(r_0,\theta,\varphi) = 1 - A(r_0)P_2(\cos\theta) + B(r_0)P_2(\lambda) + C(r_0)P_3(\lambda) + D(r_0)P_4(\lambda), \tag{A.27}$$

$$f_2(r_0,\theta,\varphi) = \frac{\partial}{\partial\theta}[A(r_0)P_2(\cos\theta) - B(r_0)P_2(\lambda) - C(r_0)P_3(\lambda) - D(r_0)P_4(\lambda)], \tag{A.28}$$

$$f_3(r_0,\theta,\varphi) = \frac{1}{\sin\theta}\frac{\partial}{\partial\varphi}[B(r_0)P_2(\lambda) + C(r_0)P_3(\lambda) + D(r_0)P_4(\lambda)]. \tag{A.29}$$

A.3. Roche potential and the gravitational acceleration

Interactions in a closed binary system are generally treated in the framework of the Roche model (Kopal 1959). We adopt the same coordinate system as the deform model. The gravitational potential which is experienced at the position $P(x,y,z)$ is the sum of the two point mass potential and the rotational potential (Huang & Taam 1990), namely,

$$\Psi = -\frac{GM_2}{(x^2+y^2)^{\frac{1}{2}}} - \frac{GM_1}{[(a-x)^2+y^2]^{\frac{1}{2}}} - \frac{1}{2}\Omega_2^2\left[\left(x - \frac{M_1}{M_1+M_2}a\right)^2 + y^2\right], \tag{A.30}$$

where a be their mutual separation. The coordinates of the position $P(x,y,z)$ can be expressed in Cartesian spherical coordinate systems. Finally, we obtain

$$\Psi(r,\theta,\varphi) = -\frac{GM_2}{r} - \frac{1}{2}\Omega_2^2 r^2\sin^2\theta - G\frac{M_1}{a}\sum_{j=2}^{4}\left(\frac{r}{a}\right)^j P_n(\lambda), \tag{A.31}$$

where χ is the angle between $\boldsymbol{a}$ and $\boldsymbol{r}$. Three components of the gravitational acceleration g_r, g_θ, and g_φ take the forms of

$$g_r = -\frac{\partial\Psi}{\partial r} = \frac{GM_2}{r^2} - \sum_{j=2}^{4}\frac{GM_1}{a^{j+1}}jr^{j-1}P_j(\lambda) - \Omega_2^2 r\sin^2\theta, \tag{A.32}$$

$$g_\theta = -\frac{\partial\Psi}{r\partial\theta} = \frac{1}{r}\left[\frac{GM_2}{a}\sum_{j=2}^{4}\left(\frac{r}{a}\right)^j P_j'(\lambda)_\theta + \Omega_2^2 r^2\sin\theta\cos\theta\right], \tag{A.33}$$

$$g_\varphi = -\frac{\partial\Psi}{r\sin\theta\partial\varphi} = \frac{1}{r\sin\theta}\frac{GM_2}{a}\sum_{j=2}^{4}\left(\frac{r}{a}\right)^j)P_j'(\lambda)_\varphi. \tag{A.34}$$

The local effective gravity is written as

$$g = \left[\left(\frac{\partial\Psi}{\partial r}\right)^2 + \left(\frac{1}{r}\frac{\partial\Psi}{\partial\theta}\right)^2 + \left(\frac{1}{r\sin\theta}\frac{\partial\Psi}{\partial\varphi}\right)^2\right]^{\frac{1}{2}}. \tag{A.35}$$

The potential of the primary star with respect to the center of the primary star can be deduced by substituting M_1 for M_2. The corresponding effective gravity can be derived with the same method. The stellar radii of two components are treated as the constant value in the Roche model. The radius is not treated as the constant value in the distorted model M1.